


# Global Approach of Tribomechanical Development of Hybrid Aluminium Matrix Syntactic Foams

Kornél Májlinger<sup>1</sup>  · Gábor Kalácska<sup>2</sup> · Imre Norbert Orbulov<sup>1,3</sup> · László Zsidai<sup>2</sup> · Benjámín Bozóki<sup>1</sup> · Róbert Keresztes<sup>2</sup>

Received: 31 August 2016 / Accepted: 7 December 2016 / Published online: 19 December 2016  
© Springer Science+Business Media New York 2016

**Abstract** Hybrid syntactic foams with AlSi12 aluminium matrix were produced by pressure infiltration. The volume ratio of iron to ceramic hollow sphere reinforcement (in the same size range) was varied, and hybrid syntactic foams were also produced with bimodal size ceramic reinforcement. Previously, a very detailed analysis of the mechanical properties of the composites was made with quasi-static compression tests, and their tribological properties were investigated by pin-on-disc method in dry and lubricated conditions. The present article establishes and clarifies the correlations between mechanical and tribological properties. The coefficient of friction, height loss of the

specimens and specific wear showed good correlation with different mechanical parameters, e.g. density, structural stiffness and yield strength. The established trends and correlations between mechanical and tribological behaviour enable a better understanding of materials design and selection for further applications of mechanically loaded sliding machine parts.

**Keywords** Metal–matrix composite · Aluminium matrix syntactic foam · Hybrid composite · Pin-on-disc testing · Dry friction · Lubricated friction · Sliding wear

---

✉ Kornél Májlinger  
vmkornel@eik.bme.hu

Gábor Kalácska  
kalacska.gabor@gek.szie.hu

Imre Norbert Orbulov  
orbulov@eik.bme.hu

László Zsidai  
zsidai.laszlo@gek.szie.hu

Benjámín Bozóki  
tucsokraj09@gmail.com

Róbert Keresztes  
keresztes.robort@gek.szie.hu

<sup>1</sup> Department of Materials Science and Engineering, Faculty of Mechanical Engineering, Budapest University of Technology and Economics, Bertalan Lajos Str. 7. MT Building, Budapest 1111, Hungary

<sup>2</sup> Institute for Mechanical Engineering Technology, Faculty of Mechanical Engineering, Szent István University, Páter Károly u. 1., Gödöllő 2103, Hungary

<sup>3</sup> MTA–BME Research Group for Composite Science and Technology, Műegyetem Rakpart 3., Budapest 1111, Hungary

## 1 Introduction

Metal matrix syntactic foams (MMSFs) originate from their polymer matrix counterparts, and they consist of a lightweight metallic matrix (usually some kind of aluminium alloy) and hollow spheres (normally ceramics or metallic). These foams are often considered as composite metallic foams (CMFs) too. MMSFs have outstanding specific properties among the porous materials. Due to the hollow spheres, their specific compressive strength and energy-absorbing capability are uniquely high [1].

The most common loading condition for MMSFs is compression (e.g. collision dampers, brake parts, anti-shock buffers, blast absorbing armours); therefore, their behaviour under compressive loading has been widely studied. For example, Gupta et al. [2–7] studied the quasi-static and high strain rate properties of various MMSF systems, such as Al–Al<sub>2</sub>O<sub>3</sub> or more unique Al–SiC MMSFs. Rabiei et al. [8–10] developed CMFs with high energy-absorbing capacity and revealed that the high strain rate and the quasi-static strain rate tests can overlap each other. Fiedler and Taherishargh et al. [11–15] produced low-density and low-cost syntactic

foams, by the combination of Al alloys and expanded perlite. The authors proved the applicability of this set of foams by numerous versatile investigations. More recently, hollow tubes were filled by their low-density MMSFs [16]. The mechanical tests of the tubes revealed high energy absorption capacity and improved mechanical stability. Lehmus and Weise et al. [17–20] and Castro et al. [21, 22] investigated high-strength, steel-based syntactic foams under different conditions and found that although the density of the produced foams is higher, it is compensated by their higher strength and energy absorption. Goel et al. [23–25] focused on the effect of strain rate on the mechanical properties. Xue et al. [26, 27] successfully applied powder metallurgy to produce Ti-based MMSFs that can be used in biomedical applications. All of the above-mentioned researches confirm that MMSFs can be produced with various matrix materials and hollow spheres and their compressive properties can be tailored to the requirements of the desired structural parts. Besides the constituents, the microstructure (detailed in [28]) and the macrostructure [29] have decisive effect on the mechanical properties. For the investigation of the applicability of MMSFs for sliding machine parts (like bearings, pistons or cylinder bores), their tribological properties should be properly investigated, and furthermore, it would be important to see the connections of mechanical properties to tribological behaviour as well. For a variety of aluminium matrix syntactic foams (AMSFs) reinforced with fly ash or cenosphere (ceramic hollow spheres) [30–38], dry wear characteristics and tribological properties were investigated with different methods; some of them are already in lubricated [30] conditions. The typical diameter of these reinforcements was less than 400  $\mu\text{m}$ , and the density of the AMSFs was bigger than 1.9  $\text{gcm}^{-3}$ . Some tribological data are available for hybrid (hollow sphere + particle) reinforced AMSFs too [39], but only a few for hollow sphere + hollow sphere reinforced hybrid AMSFs [40, 41], with larger reinforcement size ( $\theta > 1 \text{ mm}$ ). Also no literature was found in which correlations between mechanical and tribological properties of AMSFs were considered; however, in tribology, it is an essential knowledge in many aspects [42].

The main aim of our paper is to give data and broad support to: (1) further development of such porous materials in the aspect of tribological properties and (2) the successful application of AMSFs (construction, expected lifetime, etc.). As an additional feature, the properties of the AMSFs and their trends are presented in the function of their reinforcing constituents (depending on the ratio of ceramic to metallic hollow spheres). To achieve this goal, the measured tribological data of [41] and the mechanical properties of [48] were deeply analysed for correlations. The measured materials properties are detailed in the Materials and Methods section in detail.

## 2 Materials and Methods

### 2.1 Production of the AMSFs

As it was presented in detail in [41], near eutectic AlSi12 alloy was chosen for the hybrid composites as matrix material, due to its good castability.

To produce the different AMSFs, two grades of ceramic hollow spheres and one grade of metal hollow sphere reinforcement was used. The larger ceramic (commercial name: Globocer, GC) and the iron spheres (commercial name: Globomet, GM) were in the same size range (between  $\theta 1.4$  and 1.9 mm) and were provided by the same manufacturer, the Hollomet GmbH (Germany) [43], Germany. The smaller ceramic hollow spheres (commercial name: E-spheres, SLG) were produced by the EnviroSpheres Ltd. (Australia) [44]. The main properties of the matrix alloy and the hollow spheres are described in detail in [41].

To produce the AMSF blocks for further investigations, low pressure infiltration was used. The infiltration pressure was 400 kPa, the temperature was 600  $^{\circ}\text{C}$ , and the infiltration time was 15 s. This pressure infiltration set-up enables the highest reinforcement content whose theoretical value for spheres (randomly close packed) is about 64 vol% [45, 46]. More detailed description of the production method and the influence of the infiltration parameters is available in [28, 47, 48].

Two types of hybrid composites were produced with this infiltration technique. (I) The first hybrids were reinforced hollow spheres in the same size range, but with different reinforcement ratio, the GM and GC hollow sphere grades were mixed from 100% GM–0% GC to 0% GM–100% GC in 20% steps of the achievable  $\sim 64$  vol% hollow sphere content. The specimens were designated after their reinforcement ratio, e.g. 80 GM–20 GC is a hybrid AMSF containing 80 vol% GM and 20 vol% GC grade hollow spheres (of the overall 64 vol% reinforcement content). (II) Another type of hybrid AMSF was produced with bimodal reinforcement size from the ceramic SLG and GC grade reinforcements (almost identical composition, but one order of magnitude difference in the average diameter) and was designated as SLG + GC. In SLG + GC samples, the calculated ratio of SLG reinforcement between the GC spheres was about 20 vol%. AMSF with pure SLG reinforcement was also produced, for investigation of the size effect of the reinforcement.

Specimens for metallography, compressive tests and tribology tests were machined from the AMSF blocks, to avoid side effects [49]; the specimen size for mechanical and tribological tests was  $\theta 14$  mm in diameter.

According to the metallography of the produced AMSF blocks, the unwanted porosity (between the matrix material

and the hollow spheres) is negligible, but note that cracks in the wall of some spheres may occur; therefore, some of these hollow spheres were maybe filled with matrix material during infiltration process. Detailed description of the metallographic investigations and properties of these types of AMSFs was already published [28, 40, 47, 48, 50] for visualization of the microstructures; the three different grades of hollow spheres can be observed in Fig. 1. Both the small unwanted porosity and previously measured interfacial layers ( $\sim 10 \mu\text{m}$ ) indicate a good AMSF quality [48].

## 2.2 Compressive Tests of the AMSFs

As it was mentioned in the Introduction, the main load type of the MMSFs is compression, also in sliding machine components. Therefore, compressive test was performed on a MTS 810 universal materials testing machine on cylindrical samples with  $\theta 14$  mm diameter and 14 mm height. The specimens and the tools were lubricated with anti-seize material with  $\text{MoS}_2$  content. The compression tests were made in quasi-static condition with  $0.01 \text{ s}^{-1}$  deformation rate. The minimum number of 6 specimens was tested, and the average characteristic values were determined according to the DIN 50134:2008 standard. The investigated characteristic properties were the structural stiffness ( $S$ ), the fracture strain ( $\varepsilon_c$ ), the compressive strength ( $\sigma_c$ ), the yield strength ( $\sigma_y$ ), the plateau strength ( $\sigma_p$ ), the fracture energy ( $W_c$ ) and the absorbed energy ( $W_{25\%}$ ). In the compressive stress–strain curve of AMSFs (engineering system),  $S$  is the slope of the initial curve, where the whole system is deformed only elastically.  $\sigma_c$  is the stress value of the first local peak in the stress–strain curve where the breakage (ceramic) and plastic deformation (iron) of the hollow spheres begin.  $\sigma_y$  was determined at 1% plastic strain; after this stress value, the densification of the foam begins, the ceramic hollow spheres break into smaller pieces, the iron ones deform plastically, and the plastically deformed matrix material fills the hollow spaces. In this

densification region,  $\sigma_p$  was determined as the mean value between  $\varepsilon = 5\text{--}25\%$  deformation. The fracture energy ( $W_c$ ) is the integral (area under the curve) of the stress–strain curve up to the fracture strain ( $\varepsilon_c$ , as the abscissa of  $\sigma_c$ ), and the absorbed energy ( $W_{25\%}$ ) is the integral up to the end of the test ( $\varepsilon = 25\%$ ). Note that the 100 GM–0 GC specimens had no local peak in the stress–strain curve; therefore, in this case, the  $\sigma_c$  value was replaced by  $\sigma_y$  [48].

## 2.3 Pin-on-Disc Tribological Tests

For the investigation of the tribological behaviour of the produced hybrid AMSFs, pin-on-disc tests were performed. The pins were machined from the AMSF blocks with  $\varnothing 14$  mm diameter and 20 mm height. The sliding surfaces of the specimens were grinded on SiC grinding papers (till P2400 paper) under continuous water rinsing. The carbon steel counterpart disc (1.0244) was  $\theta 100$  mm, with the chemical composition of 98.4 wt% Fe, 0.221 wt% C, 0.211 wt% Si, 0.913 wt% Mn, 0.0697 wt% Cr, 0.275 wt% other. The surfaces of the discs were ground to an average surface roughness of  $R_a = 0.93 \pm 0.321 \mu\text{m}$  and  $R_z = 8.74 \pm 3.00 \mu\text{m}$  with the hardness of  $140 \pm 3$  HV10. Directly prior to the wear tests, both the surface of the specimens and the discs were cleaned with acetone and ethanol. For the tribological tests, a custom-made pin-on-disc machine [42] was used. The machine parameters were: (I) 98 N load generating 0.64 MPa nominal surface pressure and (II) sliding speed of  $0.2 \text{ m s}^{-1}$ . The tests were made in dry and lubricated conditions at ambient temperature. Before the lubrication test,  $5 \times 20 \mu\text{l}$  10W40 mineral oil was applied on the surface of the discs along the sliding track and no further lubrication was added up to the end of tests. For more details, refer to our previous paper [41]. The following parameters were determined in dry and lubricated conditions for all the AMSFs and matrix material: COF in the steady state (determined with Origin software as an average value between 300 and 500 m sliding distance) ( $\mu_{SS}$ ), specific wear in the steady state

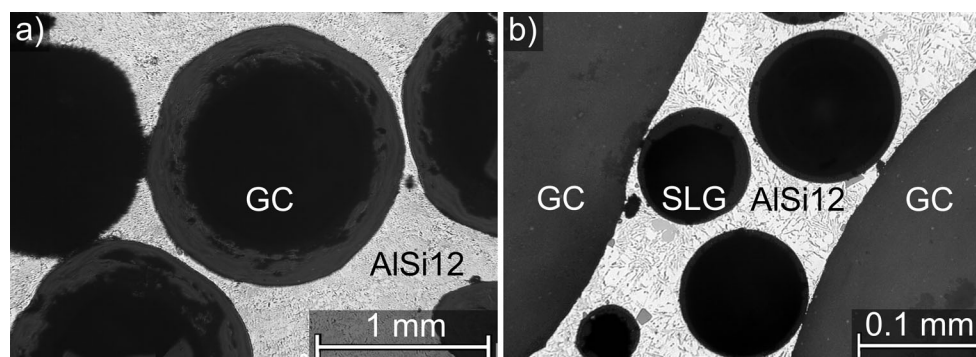


**Fig. 1** Optical microscope micrographs **a** of the 80 GM–20 GC specimens and **b** of the SLG + GC specimens microstructure

(determined between 300 and 500 m sliding distance) ( $v_{SS}$ ), overall height loss of the specimens until 500 m sliding distance ( $\Delta h_{500m}$ ) and the difference of the surface roughness of the discs ( $\Delta R_a$  and  $\Delta R_z$ ) before and after the pin-on-disc test (the  $R_a$ ,  $R_z$  values of the discs after the sliding tests were subtracted from the initial  $R_a$ ,  $R_z$  values of the discs before the tests). The surface roughness of the discs was measured with a Mitutoyo SJ-201P surface roughness tester according to the ISO 4287:1997 standard. To investigate the effect of the reinforcement size, type and ratio on the worn surfaces and subsurface areas, light microscope images were taken from the worn surfaces, and in cross section of the specimens, all the detailed metallography images and their evaluation were also introduced in our previous work [41]. In dry condition, the average wear groove depth and width ( $W_{depth}$  and  $W_{width}$ ) and also the deformed material depth ( $W_{deformed}$ ) of AMSF pin specimens were measured. Note that, in lubricated conditions, the traces of the pin were too small and shallow to measure.

In this article, we show the connection between the tribological results and the compressive mechanical properties and the density of the hybrid AMSFs for further materials design and selection.

### 3 Results and Discussion

Some correlations between different material parameters such as density, compressive properties and tribological properties were determined; the type and parameters of the correlation are all listed in Table 1. Because of the generally large scatter of the tribological data, we call “good correlation” in the cases where the coefficient of determination ( $R^2$ ) of the fitted function was above  $R^2 \geq 0.8$ ; for further evaluation, only these correlations were discussed.

#### 3.1 Mechanical Properties

The measured densities ( $\rho_{AMSF}$ ) of the AMSF blocks and the matrix material, determined by Archimedes method, are from 100 GM to 100 GC reinforcement of 1.38, 1.64, 1.65, 1.69, 1.74, 1.83  $gcm^{-3}$ ; the densities of SLG + GC, SLG and matrix material were 1.62, 1.38 and 2.65  $gcm^{-3}$ , respectively. The densities of our AMSFs are considerably lower than the similar AMSFs investigated in the literature [30–38] (where  $\rho_{AMSF} > 1.9 gcm^{-3}$ ).

The quasi-static compression tests showed significant difference in the characteristic properties of the AMSFs. Due to the higher elastic modulus of the ceramic hollow

**Table 1** Matrix of the compared mechanical and tribological parameters with indication of the ones with good correlation

Physical and mechanical properties	Dry sliding condition								Oil-lubricated condition				Density $\rho_{AMSF}$	
	COF $\mu_{SS}$	Specific wear $V_{SS}$	Height loss $\Delta h_{500m}$	Difference in surface roughness of the disc		Wear groove width $W_{width}$	Wear groove depth $W_{depth}$	Deformation depth $W_{deform.}$	COF $\mu_{SS}$	Specific wear $V_{SS}$	Height loss $\Delta h_{500m}$	Difference in surface roughness of the disc		
				$\Delta R_a$	$\Delta R_z$							$\Delta R_a$		$\Delta R_z$
Structural stiffness, $S$	+	+	+	-	-	-	-	-	+	+	-	-	-	+
Density, $\rho_{AMSF}$	-	-	+	-	-	-	-	-	+	-	-	-	-	+
Compressive strength, $\sigma_c$	-	-	-	-	-	-	-	-	+	-	-	-	-	+
Fracture strain, $\epsilon_c$	+	-	+	-	-	-	-	-	+	-	-	-	-	+
Fracture energy, $Wc$	-	-	-	-	-	-	-	-	-	-	-	-	-	+
Yield strength, $\sigma_y$	-	+	+	-	-	-	-	-	+	+	-	-	-	+
Plateau strength, $\sigma_p$	-	-	-	-	-	-	-	-	+	-	-	-	-	+
Absorbed energy, $W_{25\%}$	-	-	-	-	-	-	-	-	-	-	-	-	-	+

+ correlation ( $R^2 \geq 0.8$ )

- no correlation

spheres compared to the iron ones, the structural stiffness of the GM–GC hybrid AMSFs increased significantly with higher GC content from 2369 to 4405 MPa; the pure SLG specimen had only 2054 MPa structural stiffness, but in the SLG + GC hybrid, it increased to 4123 MPa.

The compressive strength of GM–GC hybrids increased from 35.3 to 114.5 MPa due to the greater load-bearing capability of the ceramic GC hollow spheres. The SLG foams had significantly higher compressive strength (164 MPa) due to the smaller diameter of the ceramic spheres, which decreased in case of SLG + GC foam because of the bimodal distribution of the spheres and significantly less matrix material between them. The same effect can be observed in case of yield strength and plateau strength values. The plateau strength increased from 49.3 to 88.1 MPa in case of GM–GC hybrids and decreased

from 150 MPa (SLG) to 94.8 MPa in case of SLG + GC hybrid. Also the plateau strength increased from 49.3 to 88.1 MPa in case of GM–GC hybrids and decreased from 111 MPa (SLG) to 26 MPa in case of SLG + GC hybrid.

In case of GM–GC type AMSFs, linear correlation was established between the density and structural stiffness and between the density and strength values ( $\sigma_c$ ,  $\sigma_y$  and  $\sigma_p$ ), respectively (Fig. 2a, c; Table 2).

Because of the significant increase of the strength values, the absorbed energy values also increased with the higher ceramic content (from 11.3 to 19.6 Jcm<sup>-3</sup>) in case of the GM–GC hybrids and decreased from 25.5 Jcm<sup>-3</sup> (SLG) to 9.5 Jcm<sup>-3</sup> in case of SLG + GC hybrid. In the case of GM–GC AMSFs, linear correlation was detected between the density and absorbed energy values (Fig. 2e; Table 2).

**Fig. 2** Correlations between the density and compressive properties: **a** structural stiffness, **b** fracture strain, **c** compressive strength, yield strength and plateau strength **d** fracture energy and **e** absorbed energy of the AMSFs. Note that the circled (dashed blue) SLG and SLG + GC specimens were not taken into account for the fitting (Color figure online)

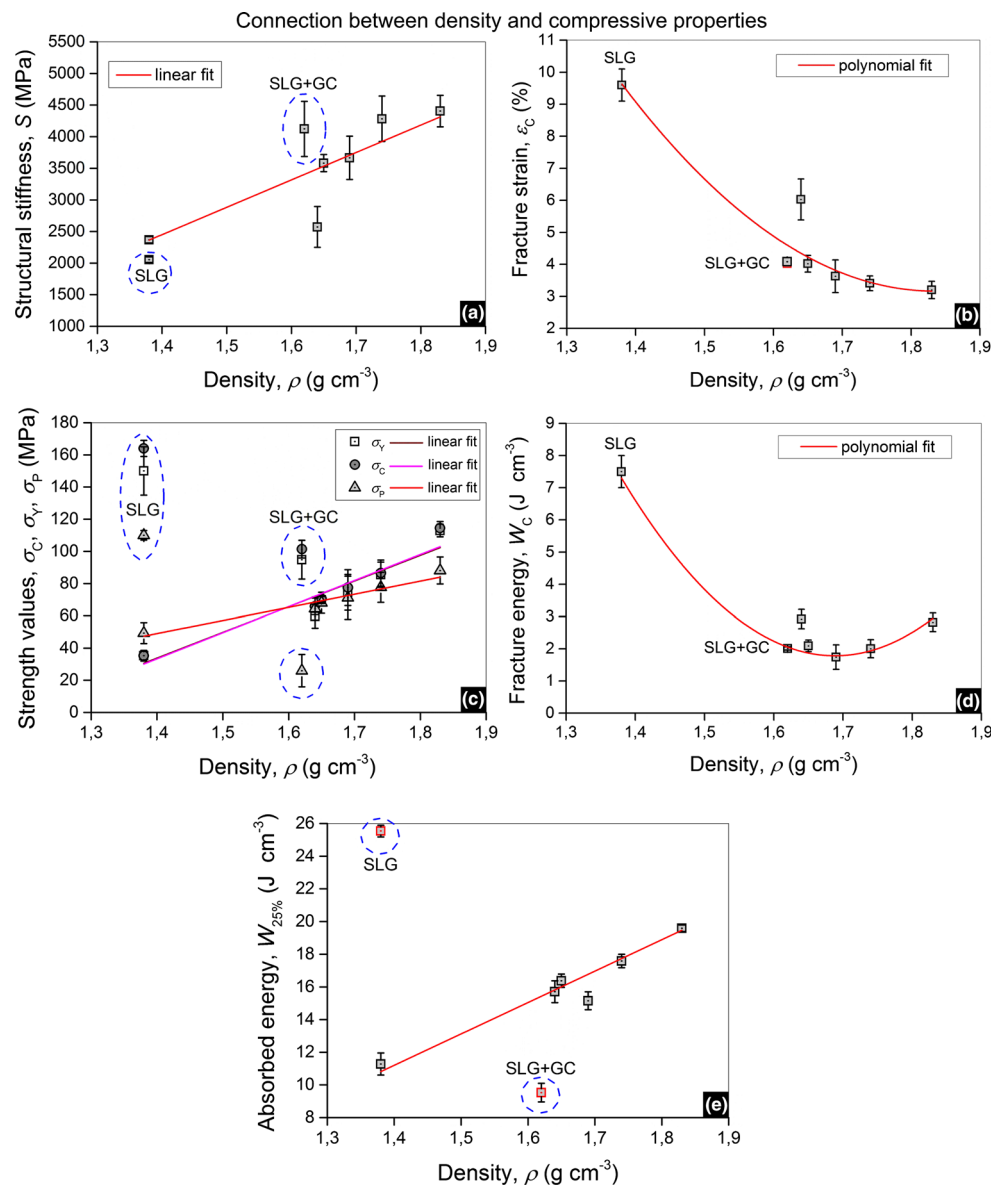




**Table 2** Equations and their parameters of the correlations between density and compressive properties, and tribological properties of the AMSFs

Parameters		Equation of the correlation	Parameters of the equation						
1	2		<i>a</i>	SE	<i>b</i>	SE	<i>y</i> <sub>0</sub>	SE	<i>R</i> <sup>2</sup>
$\rho_{\text{AMSF}}$	<i>S</i>	$Y = a + b \cdot x$	-3616.1	795.77	4332.7	548.93			0.93
$\rho_{\text{AMSF}}$	$\sigma_y$	$Y = a + b \cdot x$	-189.4	34.49	159.4	21.20			0.92
$\rho_{\text{AMSF}}$	$\sigma_c$	$Y = a + b \cdot x$	-193.3	34.69	161.9	21.28			0.92
$\rho_{\text{AMSF}}$	$\sigma_p$	$Y = a + b \cdot x$	-64.7	14.58	81.2	8.95			0.94
$\rho_{\text{AMSF}}$	$\varepsilon_c$	$y = y_0 + a \cdot x^1 + b \cdot x^2$	-114.9	35.80	31.3	10.99	108.6	29.03	0.92
$\rho_{\text{AMSF}}$	$W_c$	$y = y_0 + a \cdot x^1 + b \cdot x^2$	-196.0	34.53	58.0	10.41	167.2	28.70	0.85
$\rho_{\text{AMSF}}$	$W_{25\%}$	$Y = a + b \cdot x$	-15.7	3.80	19.2	2.17			0.94
<i>Dry condition</i>									
<i>S</i>	$\mu_{\text{SS}}$	$Y = a + b \cdot x$	0.381	0.011	$0.369 \cdot 10^{-5}$	$3.947 \cdot 10^{-6}$			0.95
<i>S</i>	$v_{\text{SS}}$	$y = a \cdot \exp(-x/b) + y_0$	-0.0308	0.019	$4.933 \cdot 10^{-5}$	$7.765 \cdot 10^{-6}$			0.87
<i>S</i>	$\Delta h_{500\text{m}}$	$y = y_0 + A / ((2\pi)^{-2} \cdot a \cdot x) \cdot \exp(-(\ln(x/b))^2 / (2a^2))$	0.261	0.046	2129	61.4	0.671	0.012	0.99
			<i>A</i>		-477.1	18.3			
$\rho_{\text{AMSF}}$	$\Delta h_{500\text{m}}$	$Y = a + b \cdot x$	-0.726	0.262	0.784	0.161			0.79
$\varepsilon_c$	$\mu_{\text{SS}}$	$y = a \cdot \exp(-x/b) + y_0$	0.432	0.322	5.659	21.1	0.301	0.702	0.83
$\varepsilon_c$	$\Delta h_{500\text{m}}$	$Y = a + b \cdot x$	0.859	0.025	-0.057	0.006			0.95
$\sigma_y$	$v_{\text{SS}}$	$y = y_0 + a \cdot x^1 + b \cdot x^2$	0.007	0.001	$-3.849 \cdot 10^{-5}$	$7.648 \cdot 10^{-6}$	-0.104	0.040	0.89
$\sigma_y$	$\Delta h_{500\text{m}}$	$y = y_0 + a \cdot x^1 + b \cdot x^2$	0.016	0.004	$-8.191 \cdot 10^{-5}$	$2.455 \cdot 10^{-5}$	-0.078	0.128	0.89
<i>Lubricated condition</i>									
<i>S</i>	$\mu_{\text{SS}}$	$Y = a + b \cdot x$	0.138	0.004	$-1.341 \cdot 10^{-5}$	$1.767 \cdot 10^{-6}$			0.90
<i>S</i>	$v_{\text{SS}}$	$y = a \cdot \exp(-x/b) + y_0$	34,006	44,440	227.4	28.3	0.065	0.021	0.99
$\rho_{\text{AMSF}}$	$\mu_{\text{SS}}$	$y = y_0 + a \cdot x^1 + b \cdot x^2$	0.537	0.329	-0.195	0.104	-0.261	0.258	0.82
$\sigma_c$	$\mu_{\text{SS}}$	$Y = a + b \cdot x$	0.124	0.006	$-4.298 \cdot 10^{-4}$	$8.103 \cdot 10^{-5}$			0.84
$\varepsilon_c$	$\mu_{\text{SS}}$	$y = a \cdot \exp(-x/b) + y_0$	-2.180	3.054	0.786	0.269	0.107	0.004	0.88
$\sigma_y$	$\mu_{\text{SS}}$	$Y = a + b \cdot x$	0.124	0.005	$-4.378 \cdot 10^{-4}$	$7.411 \cdot 10^{-5}$			0.87
$\sigma_y$	$v_{\text{SS}}$	$Y = a + b \cdot x$	1.930	0.220	-0.0254	0.003			0.91
$\sigma_p$	$\mu_{\text{SS}}$	$Y = a + b \cdot x$	0.154	0.013	$-9.123 \cdot 10^{-4}$	$1.919 \cdot 10^{-4}$			0.81

During compressive loading, the ceramic type GC and SLG hollow spheres had no plastic deformation; the AMSFs simply ruptured along a shear plane closing 45° to the loading direction (the other parts of the specimen were almost unharmed). Compared to this, the pure iron GM spheres (they are also polycrystalline with grain size <10 μm [50]) can bear large plastic deformation. This plastic deformation becomes dominant, resulting in diffuse plastic deformation of the whole specimen. It was typical in the GM–GC hybrid AMSFs from at least 80 vol% GM grade reinforcement. Therefore, the fracture strain decreased from 6 to 3.2% with increasing GC content in the GM–GC hybrids. The pure SLG specimen had larger fracture strain (9.6%)—because of the small sphere size—and it decreased with the addition of larger ceramic hollow spheres in the SLG + GC hybrid. The SLG AMSF also had the highest fracture energy and absorbed energy which decreased in the SLG + GC specimens, and in case of GM–GC hybrids, they had a minimum at 40 GM–60 GC reinforcement due to the

complex effect of the above-detailed strength and strain behaviour. A good fitting of a polynomial function was found for both density and fracture energy, and density and fracture strain values (Fig. 2b, d; Table 2).

### 3.2 Tribological Properties

From the test results of our previous work [40, 41], the following conclusions were drawn, which are the fundamentals of the present article about the trends between tribological results and material properties of AMSFs. In dry sliding conditions: (I) in case of GM–GC hybrid AMSFs, the COF increased with the ceramic reinforcement and the SLG + GC AMSF showed the highest COF. (II) In steady state, the specific wear and the overall height loss of the specimens increased with the ceramic hollow sphere content. (III) The wear type was mainly abrasive caused by the broken, hard ceramic particles (in the wear debris) besides the metallic adhesion and depended strongly on the amount and

size of ceramic particles of the broken GC and SLG hollow spheres. This ceramic particle amount increased with the higher volume fraction of GC reinforcement of the AMSFs. It was also observed that most of the larger-sized GM and GC type hollow spheres were filled with debris and plastically deformed matrix material. In oil-lubricated sliding conditions: (I) the COF was significantly less, and in case of GM–GC hybrid AMSFs, it slightly decreased with the higher ceramic reinforcement content and was less than the bulk matrix material. (II) The specific wear values were two orders of magnitude smaller; the height loss of the specimens was one order of magnitude smaller, compared to dry friction. (III) All hollow sphere grades remained open and acted as lubricant reservoirs and dispensers. The surfaces of the specimen became smoother, and the wear discs also showed no significant wear tracks.

Although the AlSi12 matrix material had less wear rate and height loss compared to the AMSFs in dry condition, in lubricated conditions the obtained values were really close to some hybrid specimen, although they have significantly less real contact surface.

The exact values of the characteristic tribological parameters determined in dry and lubricated conditions were further evaluated, and correlations between the different mechanical properties were established (Figs. 3, 4, 5 and 6).

### 3.3 Correlations Between Mechanical and Tribological Properties

The tribological parameters were plotted in the function of the compressive mechanical parameters (Figs. 3, 4, 5 and 6). With Origin software (e.g. Figs. 3 and 4 as function of the structural stiffness), correlations were searched. Table 1 lists the properties where good correlations could be found. Table 2 lists the parameters of the established correlation. The possible correlation between the mechanical and tribological properties often helps to predict the behaviour of different materials under a given condition [42].

The defined connections can be well explained on the basis of the adhesion theory of friction [51]; the dry friction force  $F_f$  is equal to the sum of adhesion ( $F_a$ ) and deformation ( $F_d$ ) components,  $F_f = F_a + F_d$ . Concerning the wear mechanism, the combination of adhesive, abrasive and third-body effects plays role. The detailed evaluations are as follows.

In Figs. 3 and 4, the significant difference between the dry and lubricated conditions of the structural stiffness—tribological parameters—can be observed.

In dry condition, the increase of the structural stiffness also increases the COF ( $\mu_{SS}$ ) and the specific wear values in the steady state ( $v_{SS}$ ). This occurred due to the fact that

under the given nominal load in the real contact zone, the deformation of the specimens with higher  $S$  values was less (more harder ceramic GC hollow spheres with greater wall thickness); therefore, besides the adhesion on the relatively smaller contact surface of the asperities, the deformation component of the less deformed microgeometry became dominant. This caused significant stress concentration in the real contact zone, which resulted in breaking off the porous specimen surface (more and more hard ceramic GC content), increasing the wear rate. The increased wear caused partially third-body abrasion also in the surface of the steel counterpart. This effect also reflected in the trends of the wear groove depth and width values determined on metallographic images. A decreasing trend (but not a good correlation) of deformed zone also can be seen because of the stiffer specimen and less contact zone.

As a function, between  $S$  and  $\mu_{SS}$  and between  $S$  and  $v_{SS}$  linear correlation was established, while between  $S$  and  $\Delta h_{500m}$  lognormal correlation was established (Tables 1, 2).

In lubricated condition, the stiffer contact zone (due to the higher ceramic hollow sphere content with higher hardness and Young modulus) was beneficial, because the porosities could hold the lubrication better with less deformation than the surfaces with less structural stiffness and therefore with larger deformation. The better lubrication caused also less contact stress and wear.

As a function, between  $S$  and  $\mu_{SS}$  linear and between  $S$  and  $v_{SS}$ , exponential decay correlation was found to fit the best (Tables 1, 2).

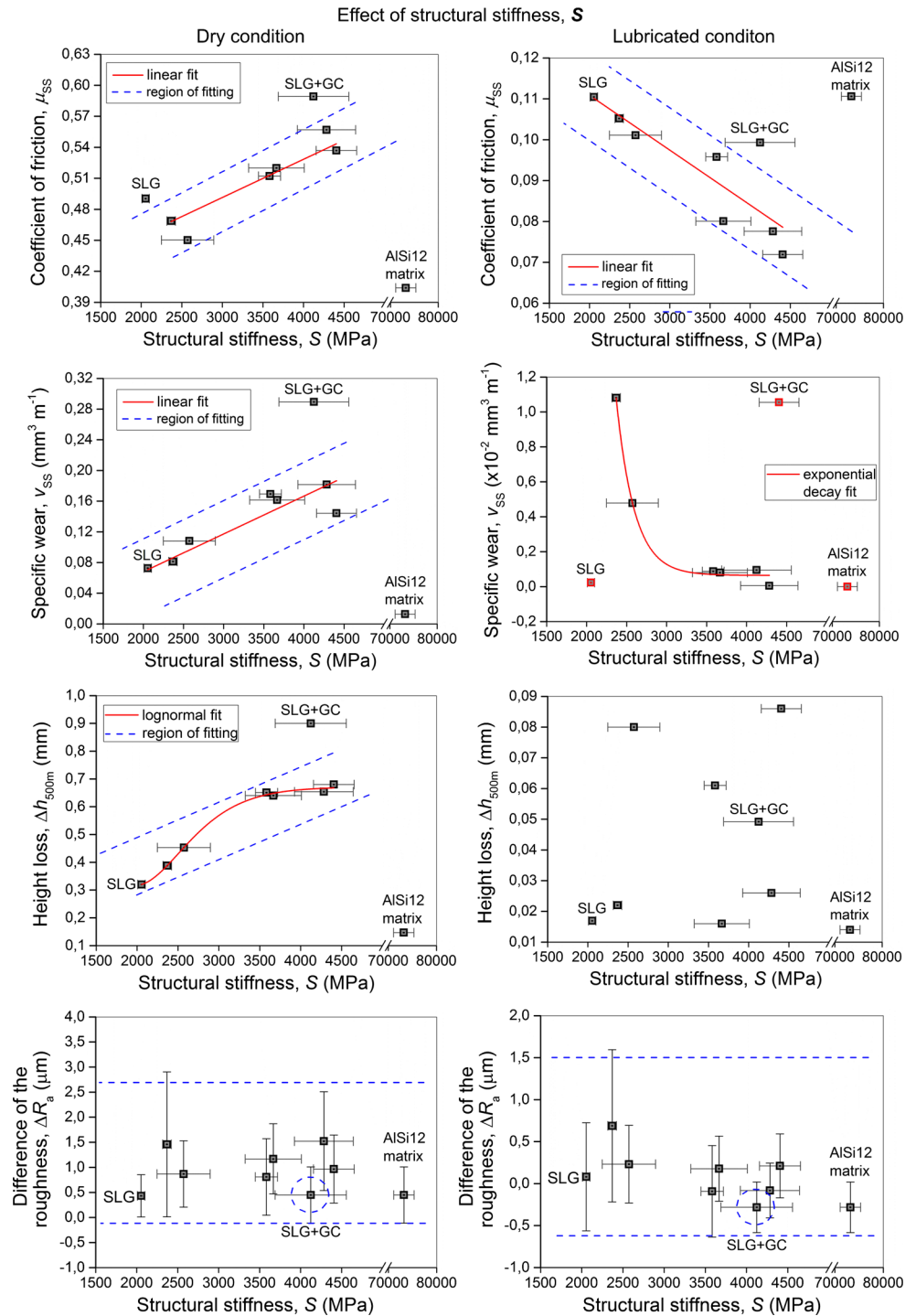
The structural stiffness had no distinctive effect on the changes in the surface roughness of the discs ( $\Delta R_a$  and  $\Delta R_z$ ) neither in dry nor in lubricated condition (Figs. 3, 4).

For further visualization, only the graphs with good correlation between mechanical and tribological parameters are plotted (Figs. 5, 6).

In case of dry sliding, a linear correlation can be observed between the density and height loss values of the GM–GC hybrids (Fig. 5a). The increasing ceramic hollow sphere content—with higher density—decreased the overall height loss. It can be explained by the resultant effect of the greater adhesion in the contact zone and the auxiliary abrasion mechanisms.

Moreover, in case of GM–GC hybrid AMSFs, the increase of the fracture strain decreased the COF (Fig. 5c): an exponential correlation was found. In the investigated system, at the given load and sliding speed the deformation component of the friction decreased because of the smaller plasticity (more GC with higher hardness, Young modulus and crush strength), while the adhesion component did not increase significantly. The increase in the fracture strain at the same time also decreased the wear and the number of detached particles from the specimens. Between  $\sigma_c$  and

**Fig. 3** Correlation between the structural stiffness and the properties of the AMSFs determined with pin-on-disc tests in dry and lubricated conditions



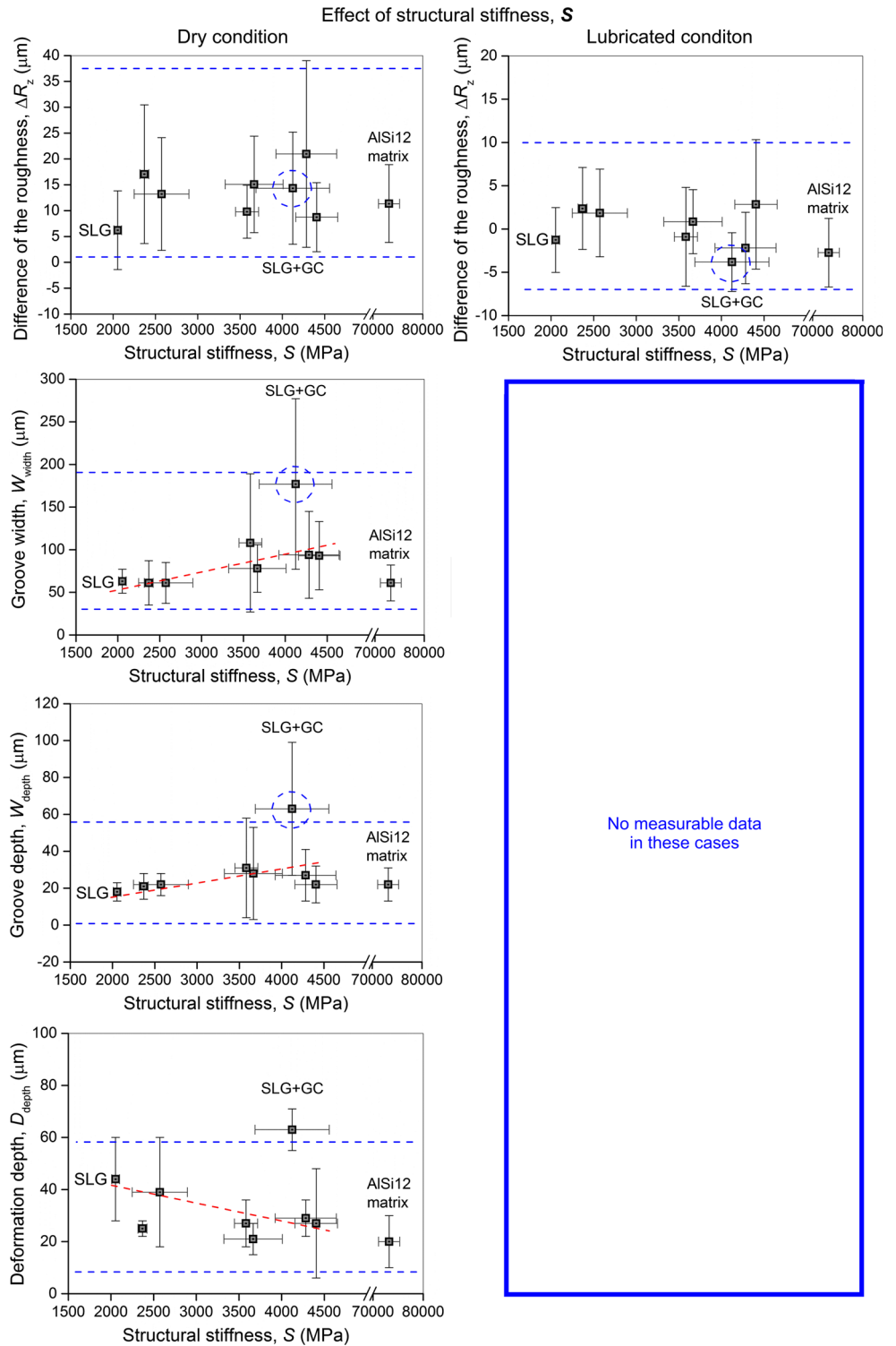
$\Delta h_{500m}$ , linear correlation was observed (Fig. 5e). In the aspect of wear, the yield strength has a distinct effect too. In case of GM–GC hybrids, the  $\sigma_c-v_{SS}$  values as well as the  $\sigma_c-\Delta h_{500m}$  showed a polynomial correlation, where the values have a maxima at about  $\sigma_c = 90$  MPa.

In oil-lubricated conditions, some correlations between tribological and mechanical properties can be established as follows (Figs. 5, 6). Investigating either

the friction or the wear, it can be confirmed that behind the detected trends, the developed, sustained and efficient lubrication is decisive. The development of an efficient lubrication is a really complex process between (different) contact surfaces with different porosity, microgeometry, adhesive aptitude and deformability. The dominant factors of the investigated systems can be observed in Figs. 5 and 6.



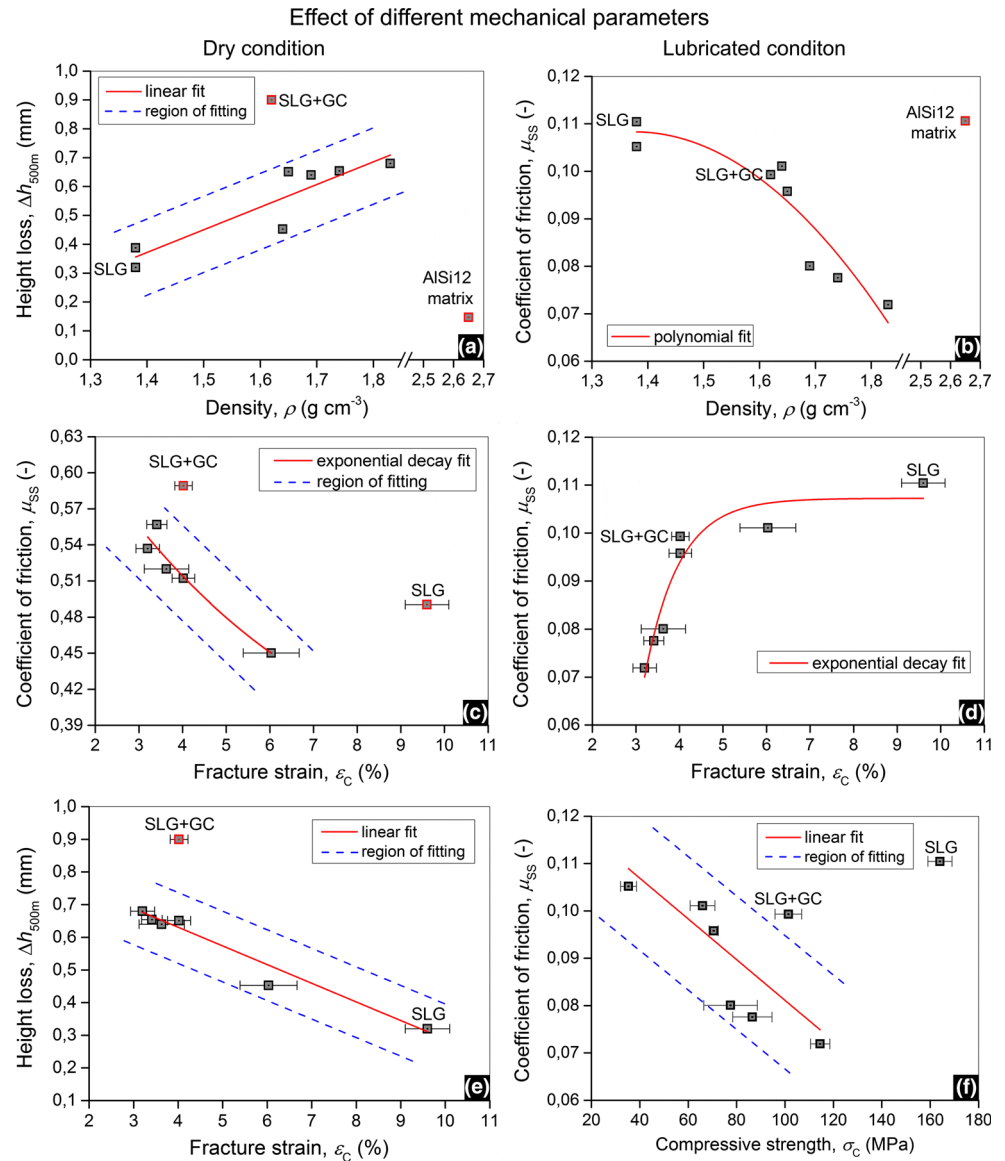
**Fig. 4** Correlation between the structural stiffness and the properties of the AMSFs determined with pin-on-disc tests in dry and lubricated conditions



The COF decreasing effect of the higher density indicates more adherent lubrication on the contact surface (on the thicker walls of the GC grade hollow spheres). A polynomial correlation between  $\rho_{\text{AMSF}}$  and  $\mu_{\text{SS}}$  was found (Fig. 5b). With increasing fracture strain, the COF also increases because of the higher deformation work (more

plastically deformable iron hollow spheres GM in the AMSFs), increasing the friction. Between  $\sigma_c$  and  $\mu_{\text{SS}}$ , exponential correlation was observed (Fig. 5d). In case of GM–GC hybrids, the increase of the yield strength decreased the resultant friction (Fig. 6b). The lubrication film minimalizes the adhesion, and the deformation

**Fig. 5** Correlation between **a**  $\rho$  and  $\Delta h_{500m}$ , **c**  $\varepsilon_c$  and  $\mu_{SS}$ , **e**  $\varepsilon_c$  and  $\Delta h_{500m}$  in dry condition and between **b**  $\rho$  and  $\mu_{SS}$ , **d**  $\varepsilon_c$  and  $\mu_{SS}$ , **f**  $\sigma_c$  and  $\mu_{SS}$  in lubricated condition



component (more hard ceramic GC hollow spheres in the AMSFs, with higher hardness yield strength) of the friction decreased with higher yield strength of the AMSFs, therefore decreasing the resultant friction. Similar observations can be made in case of yield strength-specific wear (Fig. 6d) and plateau strength-COF relations Fig. 6e. In all cases ( $\sigma_y-\mu_{SS}$ ,  $\sigma_y-\nu_{SS}$ ,  $\sigma_p-\mu_{SS}$ ), linear correlation was established for the GM-GC hybrid AMSFs.

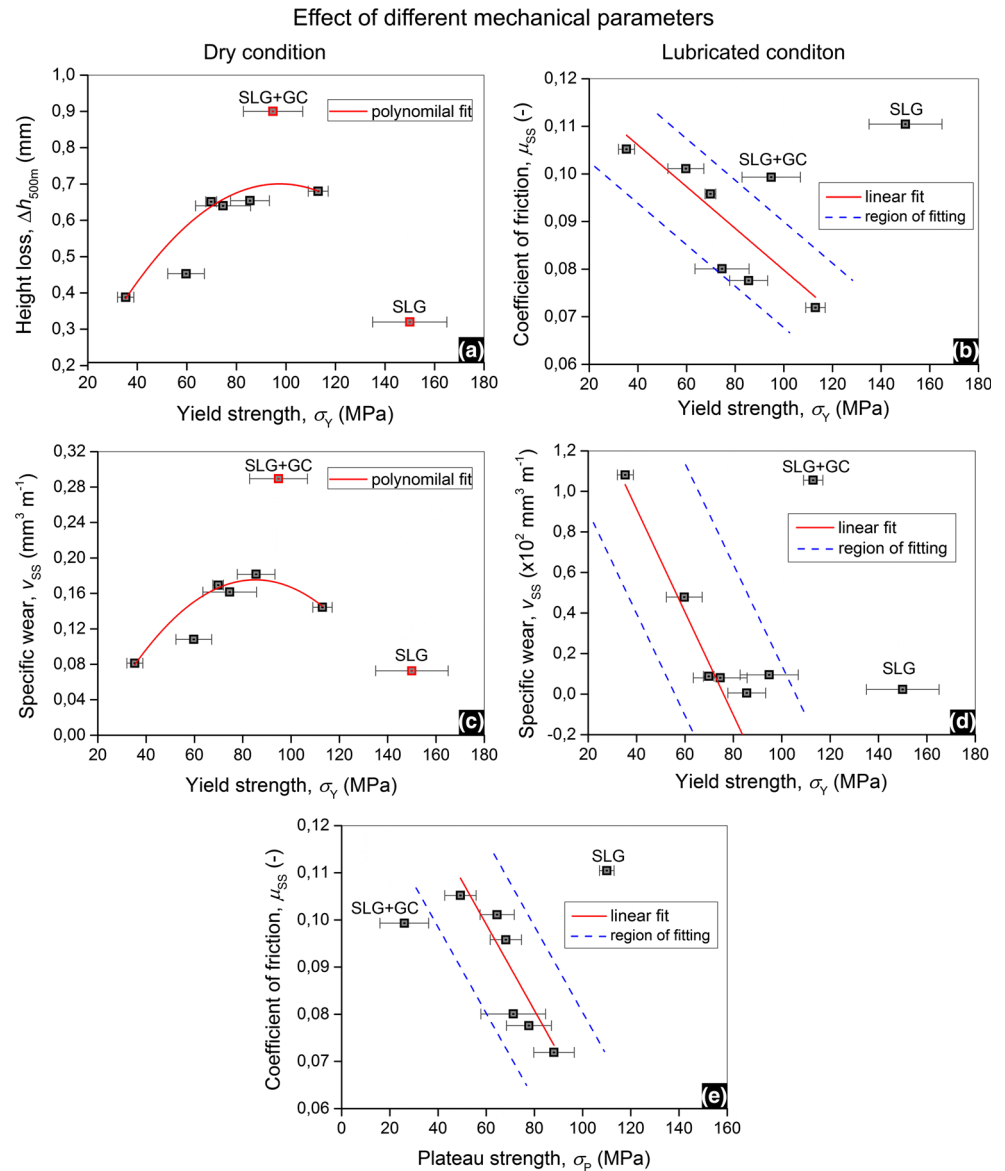
The GC + SLG hybrid specimen usually differs from the other AMSFs because of its bimodal hollow sphere distribution; the real contact surface area is a lot smaller, and there is significantly less matrix material between the different hollow spheres. Therefore, the ceramic hollow spheres can detach from the surface easier, thus increasing the third-body abrasion. Also the wall thickness differs in two orders of magnitude. In case of the SLG samples, the real contact surface is also different and the distance

between hollow sphere and matrix material (surface cavity distribution) was much less than in the case of the AMSFs reinforced with GM-GC spheres. The effects of these facts performed often strongly differ in tribological behaviour compared to GC-GM composites.

## 4 Conclusions

The previously obtained (by pin-on-disc tests) [41] tribological properties of AISi12 matrix GM-GC and SLG reinforced hybrid AMSFs were investigated in comparison with their density and quasi-static compressive properties [48]. In many cases, good correlation ( $R^2 > 0.8$ ) was found between the investigated parameters. The phenomena were explained on the complex basis of the adhesion theory of friction, the mechanical properties of composite surfaces,

**Fig. 6** Correlation between **a**  $\sigma_y$  and  $\Delta h_{500m}$ , **c**  $\sigma_y$  and  $v_{SS}$  in dry condition and between **b**  $\sigma_y$  and  $\mu_{SS}$ , **d**  $\sigma_y$  and  $v_{SS}$ , **e**  $\sigma_p$  and  $\mu_{SS}$  in lubricated condition



the adhesive and abrasive wear mechanism altogether. From the test results and in the aspect of materials selection for mechanically loaded sliding machine parts, the following conclusions can be drawn:

- In case of GM–GC AMSFs, density correlated linearly with the structural stiffness, the fracture strength, the yield strength, the plateau strength and the absorbed energy values, respectively. A good polynomial correlation of second degree was also found between the density and fracture strain and between the density and fracture energy values. All of the before-mentioned properties increased with higher density, except the fracture strain and absorbed energy values.

As for the correlations with tribological properties in dry sliding conditions:

- With higher structural stiffness of the AMSFs, the COF and specific wear increased linearly and the overall height loss increased with a lognormal function.
- With higher density, the overall height loss increased linearly.
- With higher fracture strain values, the COF decreased exponentially and the overall height loss decreased linearly.
- Between the yield strength–height loss and specific wear values, a second-order polynomial correlation was established.

As for the correlations with tribological properties in oil-lubricated sliding conditions:

- In case of GM–GC AMSFs with higher structural stiffness, the COF decreased linearly, while the specific wear decreased exponentially.

- A second-order polynomial decrement was established in the COF with higher AMSFs density.
- Higher fracture strain increased the COF exponentially.
- In the case of GM–GC AMSFs with higher strength values (compressive, yield and plateau strength too), the COF decreased linearly.
- With higher yield strength, the specific wear decreased linearly in case of the GM–GC hybrids.

The GC + SLG hybrid samples significantly differ from the other AMSFs and therefore usually showed different tribological and mechanical properties. The main reason of this phenomenon can be found in their bimodal hollow sphere distribution. In this case, the real contact surface area is a lot smaller and there is a significantly less matrix material between the different hollow spheres.

Altogether these results enlighten the basic trends and correlations between mechanical and sliding characteristics of hybrid composites and enable to tailor not only the mechanical but also the tribological properties as well for further development and application of AMSFs.

**Acknowledgements** This paper was supported by the János Bolyai Research Scholarship of the Hungarian Academy of Sciences (L. Zsidai, Grant Number: BO/00127/13/6 and I.N. Orbulov, Grant Number: BO/00294/14).

## References

- Gupta, N., Rohatgi, K.P.: Metal Matrix Syntactic Foams, p. 352. DEStech Publications, Inc., Lancaster (2014). ISBN 978-1-932078-83-1
- Luong, D.D., Strbik, O.M., Hammond, V.H., Gupta, N., Cho, K.: Development of high performance lightweight aluminum alloy/SiC hollow sphere syntactic foams and compressive characterization at quasi-static and high strain rates. *J. Alloys Compd.* **550**, 412 (2013). doi:10.1016/j.jallcom.2012.10.171
- Santa Maria, J.A., Schultz, B.F., Ferguson, J.B., Guptan, N., Rohatgi, P.K.: Effect of hollow sphere size and size distribution on the quasi-static and high strain rate compressive properties of Al-A380-Al2O3 syntactic foams. *J. Mater. Sci.* **49**, 1267 (2014). doi:10.1007/s10853-013-7810-y
- Rohatgi, P.K., Gupta, N., Schultz, B.F., Luong, D.D.: The synthesis, compressive properties, and applications of metal matrix syntactic foams. *JOM* **63**(2), 36 (2011). doi:10.1007/s11837-011-0026-1
- Luong, D.D., Gupta, N., Daoud, A., Rohatgi, P.K.: High strain rate compressive characterization of aluminum alloy/fly ash cenosphere composites. *JOM* **63**(2), 53 (2011). doi:10.1007/s11837-011-0029-y
- Luong, D.D., Gupta, N., Rohatgi, P.K.: The high strain rate compressive response of Mg–Al alloy/fly Ash cenosphere composites. *JOM* **63**(2), 48 (2011). doi:10.1007/s11837-011-0028-z
- Cox, J., Luong, D.D., Shunmugasamy, V.C., Gupta, N., Strbik, I.I.O.M., Cho, K.: Dynamic and thermal properties of aluminum alloy A356/silicon carbide hollow particle syntactic foams. *Metals* **4**, 530 (2014). doi:10.3390/met4040530
- Rabiei, A., Garcia-Avila, M.: Effect of various parameters on properties of composite steel foams under variety of loading rates. *Mater. Sci. Eng., A* **564**, 539 (2013). doi:10.1016/j.msea.2012.11.108
- Alvandi-Tabrizi, Y., Whisler, D.A., Kim, H., Rabiei, A.: High strain rate behavior of composite metal foam. *Mater. Sci. Eng., A* **631**, 248 (2015). doi:10.1016/j.msea.2015.02.027
- Alvandi-Tabrizi, Y., Rabiei, A.: Use of composite metal foam for improving absorption of collision forces. *Procedia Mater. Sci.* **4**, 377 (2014). doi:10.1016/j.mspro.2014.07.577
- Taherishargh, M., Belova, I.V., Murch, G.E., Fiedler, T.: Low-density expanded perlite-aluminium syntactic foam. *Mater. Sci. Eng., A* **64**, 127 (2014). doi:10.1016/j.msea.2014.03.003
- Taherishargh, M., Belova, I.V., Murch, G.E., Fiedler, T.: On the mechanical properties of heat-treated expanded perlite–aluminium syntactic foam. *Mater. Des.* **63**, 375 (2014). doi:10.1016/j.matdes.2014.06.019
- Taherishargh, M., Sulong, M.A., Belova, I.V., Murch, G.E., Fiedler, T.: On the particle size effect in expanded perlite aluminium syntactic foam. *Mater. Des.* **66**, 294 (2015). doi:10.1016/j.matdes.2014.10.073
- Taherishargh, M., Belova, I.V., Murch, G.E., Fiedler, T.: Pumice/aluminium syntactic foam. *Mater. Sci. Eng., A* **635**, 102 (2015). doi:10.1016/j.msea.2015.03.061
- Fiedler, T., Taherishargh, M., Krstulović-Opara, L., Vesenjak, M.: Dynamic compressive loading of expanded perlite/aluminum syntactic foam. *Mater. Sci. Eng., A* **626**, 296 (2015). doi:10.1016/j.msea.2014.12.032
- Taherishargh, M., Vesenjak, M., Belova, I.V., Krstulović-Opara, L., Murch, G.E., Fiedler, T.: In situ manufacturing and mechanical properties of syntactic foam filled tubes. *Mater. Des.* **99**, 356 (2016). doi:10.1016/j.matdes.2016.03.077
- Weise, J., Lehnhus, D., Baumeister, J., Kun, R., Bayoumi, M., Busse, M.: Production and properties of 316L stainless steel cellular materials and syntactic foams. *Steel Res. Int.* **85**(3), 486 (2014). doi:10.1002/srin.201300131
- Peroni, L., Scapin, M., Avalle, M., Weise, J., Lehnhus, D.: Dynamic mechanical behavior of syntactic iron foams with glass microspheres. *Mater. Sci. Eng., A* **522**, 364 (2012). doi:10.1016/j.msea.2012.05.053
- Lehnhus, D., Weise, J., Baumeister, J., Peroni, L., Scapin, M., Fichera, C., Avalle, M., Busse, M.: Quasi-static and dynamic mechanical performance of glass microsphere- and cenosphere-based 316L syntactic foams. *Procedia Mater. Sci.* **4**, 383 (2014). doi:10.1016/j.mspro.2014.07.578
- Peroni, L., Scapin, M., Fichera, C., Lehnhus, D., Weise, J., Baumeister, J., Avalle, M.: Investigation of the mechanical behaviour of AISI 316L stainless steel syntactic foams at different strain-rates. *Compos. Part B* **66**, 430 (2014). doi:10.1016/j.compositesb.2014.06.001
- Castro, G., Nutt, S.R.: Synthesis of syntactic steel foam using gravity-fed infiltration. *Mater. Sci. Eng. A Struct.* **553**, 89 (2012). doi:10.1016/j.msea.2012.05.097
- Castro, G., Nutt, S.R.: Synthesis of syntactic steel foam using mechanical pressure infiltration. *Mater. Sci. Eng., A* **535**, 274 (2012). doi:10.1016/j.msea.2011.12.084
- Goel, M.D., Peroni, M., Solomos, G., Mondal, D.P., Matsagar, V.A., Gupta, A.K., Larcher, M., Marburg, S.: Dynamic compression behavior of cenosphere aluminum alloy syntactic foam. *Mater. Des.* **42**, 418 (2012). doi:10.1016/j.matdes.2012.06.013
- Goel, M.D., Mondal, D.P., Yadav, M.S., Gupta, A.K.: Effect of strain rate and relative density on compressive deformation behavior of aluminum cenosphere syntactic foam. *Mater. Sci. Eng., A* **590**, 406 (2014). doi:10.1016/j.msea.2013.10.048
- Goel, M.D., Matsagar, V.A., Gupta, A.K., Marburg, S.: Strain rate sensitivity of closed cell aluminum fly ash foam. *Trans. Nonferrous Met. Soc. China* **23**(4), 1080 (2013). doi:10.1016/S1003-6326(13)62569-8

26. Xue, X.-B., Wang, L.-Q., Wang, M.-M., Lü, W.-J., Zhang, D.: Manufacturing, compressive behaviour and elastic modulus of Ti matrix syntactic foam fabricated by powder metallurgy. *Trans. Nonferrous Met. Soc. China* **22**, 188 (2012). doi:[10.1016/S1003-6326\(12\)61707-5](https://doi.org/10.1016/S1003-6326(12)61707-5)
27. Xue, X.-B., Zhao, Y.: Ti matrix syntactic foam fabricated by powder metallurgy: particle breakage and elastic modulus. *JOM* **63**(2), 43 (2011). doi:[10.1007/s11837-011-0027-0](https://doi.org/10.1007/s11837-011-0027-0)
28. Orbulov, I.N., Májlinger, K.: Microstructural aspects of ceramic hollow microspheres reinforced metal matrix composites. *Int. J. Mater. Res.* **9**, 903 (2013). doi:[10.3139/146.110944](https://doi.org/10.3139/146.110944)
29. Kozma, I., Zsoldos, I., Dorogi, G., Papp, S.: Computer tomography based reconstruction of metal matrix syntactic foams. *Period. Polytech. Mech. Eng.* **58**, 87 (2014). doi:[10.3311/PPme.7337](https://doi.org/10.3311/PPme.7337)
30. Rohatgi, P.K., Guo, R.Q.: Mechanism of abrasive wear of Al–Si hypoeutectic alloy containing 5 vol% fly ash. *Tribol. Lett.* **3**, 339 (1997). doi:[10.1023/a:1019109911923](https://doi.org/10.1023/a:1019109911923)
31. Ramachandra, M., Radhakrishna, K.: Synthesis-microstructure-mechanical properties-wear and corrosion behavior of an Al–Si (12%): flyash metal matrix composite. *J. Mater. Sci.* **40**, 5989 (2005). doi:[10.1007/s10853-005-1303-6](https://doi.org/10.1007/s10853-005-1303-6)
32. Ramachandra, M., Radhakrishna, K.: Effect of reinforcement of flyash on sliding wear, slurry erosive wear and corrosive behavior of aluminium matrix composite. *Wear* **262**, 1450 (2007). doi:[10.1016/j.wear.2007.01.026](https://doi.org/10.1016/j.wear.2007.01.026)
33. Mondal, D.P., Das, S., Jha, N.: Dry sliding wear behaviour of aluminum syntactic foam. *Mater. Des.* **30**, 2563–2568 (2009). doi:[10.1016/j.matdes.2008.09.034](https://doi.org/10.1016/j.matdes.2008.09.034)
34. Uthayakumar, M., Kumaran, S.T., Aravindan, S.: Dry sliding friction and wear studies of fly ash reinforced AA-6351 metal matrix composites. *Tribol. Adv* (2013). doi:[10.1155/2013/365602](https://doi.org/10.1155/2013/365602)
35. Sudarshan, M.K.S.: Dry sliding wear of fly ash particle reinforced A356 Al composites. *Wear* **265**, 349 (2008). doi:[10.1016/j.wear.2007.11.009](https://doi.org/10.1016/j.wear.2007.11.009)
36. Saravanan, V., Thyla, P.R., Balakrishnan, S.R.: The dry sliding wear of cenosphere-aluminum metal matrix composite. *Adv. Compos. Lett.* **23**(3), 49 (2015)
37. Kumar, K.A.R., Balamurugan, K., Gnanaraj, D.: Hardness, tribology and microstructural studies on aluminium: flyash metal matrix composites. *J. Sci. Ind. Res.* **74**(3), 165 (2015)
38. Kumar, V., Gupta, R.D., Batra, N.K.: Comparison of mechanical properties and effect of sliding velocity on wear properties of Al 6061, Mg 4%, fly ash and Al 6061, Mg 4%, graphite 4%, fly ash hybrid metal matrix composite. *Procedia Mater. Sci.* **6**, 1365 (2014). doi:[10.1016/j.mspro.2014.07.116](https://doi.org/10.1016/j.mspro.2014.07.116)
39. Muthu, P., Rajesh, S.: Dry sliding wear behaviour of aluminum/flyash hybrid metal matrix composites. *J. Aust. Ceram. Soc.* **52**(1), 125 (2016)
40. Májlinger, K.: Wear properties of hybrid AlSi12 matrix syntactic foams. *Int. J. Mater. Res.* **106**(11), 1165 (2015). doi:[10.3139/146.111290](https://doi.org/10.3139/146.111290)
41. Májlinger, K., Bozóki, B., Kalácska, G., Keresztes, R., Zsidai, L.: Tribological properties of hybrid aluminum matrix syntactic foams. *Tribol. Int.* **99**, 211 (2016). doi:[10.1016/j.triboint.2016.03.032](https://doi.org/10.1016/j.triboint.2016.03.032)
42. Kalácska, G.: An engineering approach to dry friction behaviour of numerous engineering plastics with respect to the mechanical properties. *Exp. Polym. Lett.* **7**(2), 199 (2013). doi:[10.3144/expresspolymlett.2013.18](https://doi.org/10.3144/expresspolymlett.2013.18)
43. <http://hollomet.com/produkte.html>. Accessed 10 Aug 2014
44. [http://www.envirospheres.com/products\\_bl.asp](http://www.envirospheres.com/products_bl.asp). Accessed 10 March 2015
45. Jaegerand, H.M., Nagel, S.R.: Physics of the granular state. *Science* **255**, 1523 (1992). doi:[10.1126/science.255.5051.1523](https://doi.org/10.1126/science.255.5051.1523)
46. Torquato, S., Truskett, T.M., Debenedetti, P.G.: Is random close packing of spheres well defined? *Phys. Rev. Lett.* **84**, 2064 (2000). doi:[10.1103/PhysRevLett.84.2064](https://doi.org/10.1103/PhysRevLett.84.2064)
47. Orbulov, I.N.: Metal matrix syntactic foams produced by pressure infiltration: the effect of infiltration parameters. *Sci. Eng. A, Mater* (2013). doi:[10.1016/j.msea.2013.06.066](https://doi.org/10.1016/j.msea.2013.06.066)
48. Májlinger, K., Orbulov, I.N.: Characteristic compressive properties of hybrid metal matrix syntactic foams. *Mater. Sci. Eng., A* **606**, 248 (2014). doi:[10.1016/j.msea.2014.03.100](https://doi.org/10.1016/j.msea.2014.03.100)
49. Ashby, M.F., Evans, A.G., Fleck, N.A., Gibson, L.J., Hutchinson, J.W., Wadley, H.N.G.: *Metal Foams: A Design Guide*. Butterworth-Heinemann, Boston (2010). ISBN 0750672196
50. Szlancsik, A., Katona, B., Májlinger, K., Orbulov, I.N.: Compressive behavior and microstructural characteristics of iron hollow sphere filled aluminum matrix syntactic foams. *Materials* **8**(11), 7926 (2015). doi:[10.3390/ma8115432](https://doi.org/10.3390/ma8115432)
51. Bowden, F.P., Tabor, D.: *Friction and Lubrication of Solids*. Oxford University Press, London (1954). ISBN 9780198507772